Low Noise Transition Edge Sensor (TES) for the SAFARI Instrument on SPICA

P. Khosropanah, R.A. Hijmering, M. Ridder, M.A. Lindeman, L. Gottardi, M. Bruijn, J. van der Kuur, P.A.J. de Korte, J.R. Gao, H. Hoevers

***Abstract*—We fabricated and characterized a low thermal conductance (*G*) transition edge sensor (TES). The device is based on a superconducting Ti/Au bilayer deposited on a suspended SiN membrane. The critical temperature of the device is 78 mK. The low thermal conductance is realized by using narrow SiN supporting structures. All measurements were performed having the device in a light-tight box, which to a great extent eliminates the loading of the background radiation. We measured the current-voltage (IV) characteristics of the device at different bath temperatures and determine the thermal conductance (*G*) to be equal to 0.13 pW/K. The current noise and complex impedance are also measured at different bias points at a bath temperature of 30 mK. The measured electrical (dark) NEP is 4.2×10^{-19} W/√Hz, which is about a factor of 3 higher than what is expected from the thermal conductance that comes out of the IV curves analysis. We also measured the complex impedance of the same device at several bias points. Fitting a simple first order thermal-electrical model to the measured data, we find an effective time constant of about 1-4.5 ms and a heat capacity of 2-3 fJ/K.**

***Index Terms*—Transition-edge sensor, TES, far infra-red spectrometer, submm spectrometer, SiN membrane.**

I. INTRODUCTION

SPICA [1] is a Japanese-led mission to fly a 3.5 m diameter IR telescope with a cryogenically cooled mirror (~5K). Cooling the optics reduces the background radiation caused by the ambient temperature of the telescope that limits the sensitivity. The loading is then dominated by astrophysical background sources. SAFARI [2] is the European instrument on SPICA. It is an imaging Fourier Transform Spectrometer (FTS) with three bands in the wavelength ranges: 35-60 μm, 60-110 μm and 110-210 μm. The loading in these bands is dominated by emission from the Zodiacal light at a level of 0.3-1 fW [2]. This gives a photon noise equivalent power (NEP) at the detectors of $1\text{-}3\times10^{-18}$ W/√Hz. We require detectors with electrical NEP at least 3 times lower than the photon noise limit, i.e. $\leq 3\times10^{-19}$ W/√Hz. This sensitivity is about 2 orders of magnitude higher than what is required for detectors on a ground based telescope, imposing a great challenge on the detector technology. The requirement for the response time of the detectors for SAFARI is set to $\tau \leq 8$ ms, determined by the maximum scanning speed of the FTS mechanism and the downlink bandwidth.

A transition edge sensor (TES) is the selected detector technology for the SAFARI. Silicon nitride suspended structures (although not for TES) were originally developed for ground-based mm-wave observations and have been used in a large number of ground-based and sub-orbital experiments [3]-[6]. Silicon nitride suspended structures were used in the Herschel-SPIRE [7] and the Planck space observatory [8]. All of the detectors in these instruments use bolometer chips that are bonded to the silicon nitride membranes in a hybrid process [9]-[10]. More recently, a number of groups have developed bolometers incorporating silicon nitride thermal isolation combined with TES bolometers (see Ref. [11] and references therein).

In collaboration with several European TES groups, SRON is developing low thermal conductance TES bolometers for SAFARI. These devices are based on a Ti/Au superconducting bilayer as the sensitive element on a suspended silicon nitride membrane.

Previously we reported measurements of a single pixel TES using long diagonal legs [12]. Also the optical test of a similar TES integrated with an absorber was reported [13], where the radiation is coupled to the detector using a conical horn. In order to achieve very low thermal conductance we needed to use 4 very long diagonal legs of 1800 μm. This makes the detector size rather large and therefore not suitable for making arrays with required pixel pitch size for the SAFARI. One solution to overcome this problem is to make ring-like supporting structure [14]. In this paper an alternative approach is taken by having the TES supported by tilted parallel legs.

We present the details of the detector and electrical (dark) characterization, including IVs, noise, impedance data and the analysis.

II. TES DEVICE

The device under test is based on a Ti/Au (16/60 nm) bilayer, deposited on 0.5 μm thick suspended SiN membrane. The TES area is 50×50 μm^2 and the critical temperature (T_C) is 78 mK. In order to be able to test this device optically (not reported here), we have an absorber close to the TES, which is an 8 nm thick Ta with an area of 70×70 μm^2. The absorber and the TES are sitting on a 130×70 μm^2 SiN island.

Fig. 1 shows a picture of the device. There are 4 SiN supporting legs that are 2 μm wide and 2000 μm long. The

Manuscript received 1 August 2011. This work is supported in part by ESA TRP contract: ITT-1-5922/08/NL/EM TES spectrometer.

P. Khosropanah, M. Ridder, R. Hijmering, J. van der Kuur, L. Gottardi, M. Bruijn, M. Popescu, J. R. Gao, H. Hoevers are with the SRON Netherlands Institute for Space Research, Sorbonnelaan 2, 3584 CA Utrech, the Netherlands (phone: +31-88877-5600; fax: +31-888-77 5601; email: P.Khosropanah@sron.nl).

J. R. Gao is also with Kavli Institute of NanoScience, Delft University of Technology, Delft, the Netherlands.

electrical contact to the bolometer is realized by 90 nm thick Nb wiring on the top of SiN legs.

Similar devices are fabricated in an array of 5×5 with a pitch size of 840 μm, which is required by the SAFARI long wavelength focal plane array (see Fig. 2).

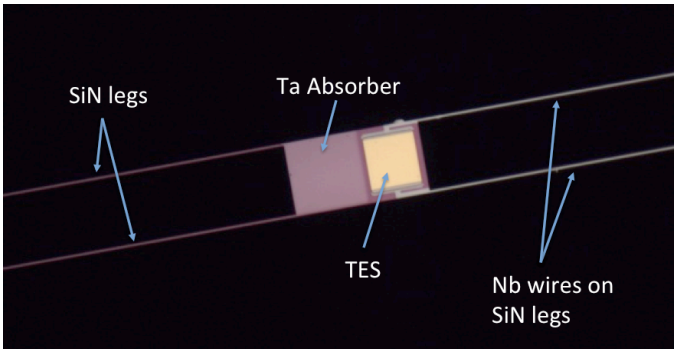

Fig. 1. TES on suspended SiN structure with a spider-web-like design. In the middle of each detector there is a TES and an absorber on a SiN membrane.

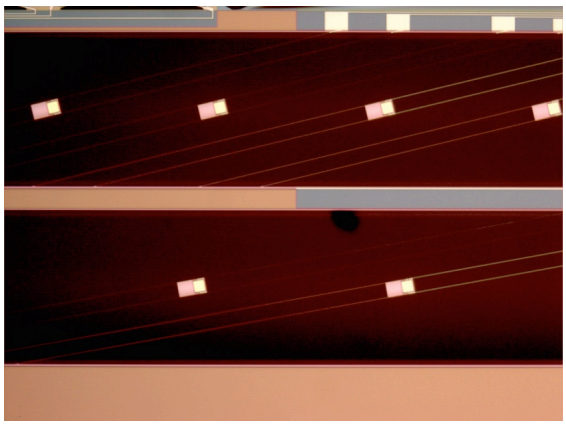

Fig. 2. TES array on suspended SiN structure with tilted parallel legs design. By increasing the tilt angel the leg length increases while the pitch size stays the same.

III. Current-Voltage Characteristics

The detector is tested using a Kelvinox dilution fridge with a base temperature of 16 mK. The detector is mounted in a light tight box, which is designed to minimize the background loading due to possible stray light. The electrical wiring into this box goes through a meander path that is filled with Stycast mixed with SiC grains.

The biasing is done by using a *dc* current source in parallel with 5 mΩ shunt resistance that simulates a voltage bias. The current in the TES is read out using a SQUID with a closed flux locked loop. Fig. 3 shows a set of measured IV curves at bath temperatures varying from 30 to 70 mK. The *dc* power in the transition at each bath temperature is almost constant. Fig. 4 shows the power level as a function of bath temperature.

The heat flow equation for a TES can be written as:

$$P = K(T_C^{\ n} - T_{bath}^{\ n}), \quad (2)$$

where P is the bias power applied to the TES; K a constant that depends on the geometry and material properties of the supporting legs; T_C the critical temperature of the bilayer; and T_{bath} the bath temperature. All parameters are known in (2) except for n and K, we can fit (2) to the measured data to find both values. For this device the best fit was obtain using $n = 2.5$ and $K = 2.66$ pW/K^n. The fundamental phonon noise in TES can be written as [15]:

$$NEP = \sqrt{\gamma 4 k_B T^2 G}, \quad (3)$$

where γ is a number between 0.5 and 1 that accounts for temperature gradient along the supporting legs and in our case is about 0.5, k_B is the Boltzmann's constant, T is the temperature of the TES, which is equal to T_C, and G is the thermal conductance between the TES and the substrate which can be written as:

$$G = nKT_C^{n-1}. \quad (4)$$

Inserting the values from the fit in Fig. 4 gives a G of 0.13 pW/K, which in turn results in an expected dark NEP of 1.4×10^{-19} W/√Hz using (3).

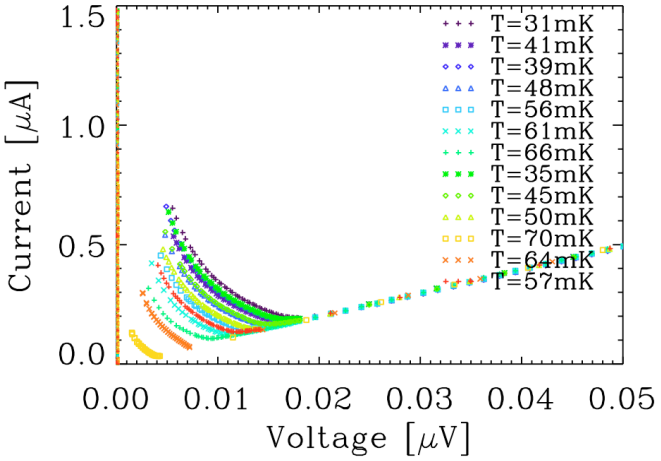

Fig. 3. Calibrated IV curves at different bath temperature.

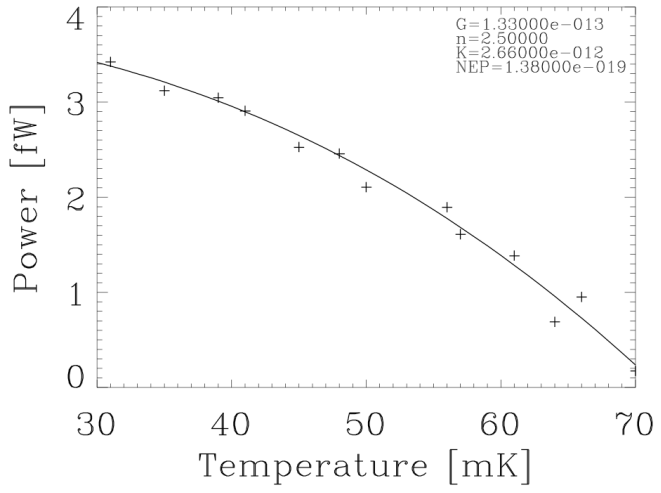

Fig. 4. Power plateaus in the transition as a function of bath temperature.

IV. Noise Measurement

Fig. 5 shows the measured current noise spectra at several bias points in the transition at a bath temperature of 30 mK. The data have a frequency resolution of 1 Hz. Dividing the current noise by the responsivity yields the electrical (dark) NEP at each operating point. The responsivity at low

frequencies can be approximated by $\frac{1}{I_0(R_0 - R_{Th})}$, where I_0 is the bias current, R_0 is the resistance of TES and R_{Th} is the Thevenin resistance in the bias circuit that is $R_{series}+R_{shunt}$. The dark NEP at low frequency at all points in the transition is about 4.2×10^{-19} W/√Hz, which is a factor of 3 higher than what we expect from the measured G. We believe that the main part of this excess noise is due to the thermal fluctuations in the long legs.

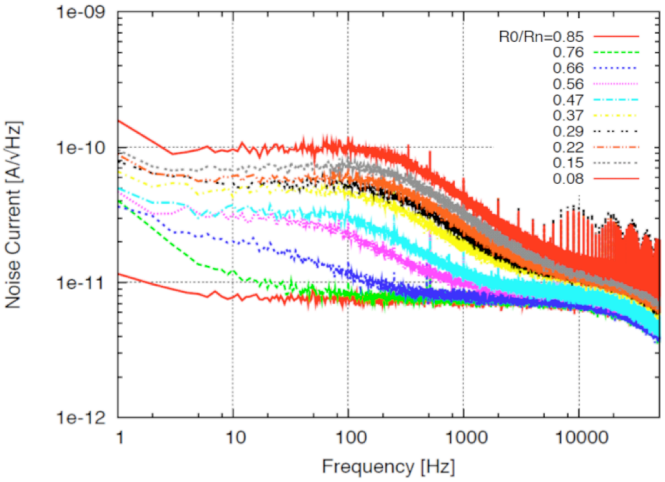

Fig. 5. Noise current spectra measured at a bath temperature of 30 mK in the transition that corresponds to NEP= 4.2×10^{-19} W/√Hz. R_0 is the TES resistance at the bias point where the noise was measured and R_n is the normal state resistance of the device.

V. TES Speed

The speed of the device at different bias points is measured by applying a small step current (less than 10% of the bias current) and recording the output signal. Since the signal is small it has to be averaged for over 500 times. The curves are then fit by a first order exponential function that gives the time constant of the response. Fig. 6 shows the measured curves and the fits. The effective time constant varies between 4.5 ms at high in the transition to 1 ms at low in the transition. These numbers are well within SAFARI specifications that require $\tau \leq 8$ ms.

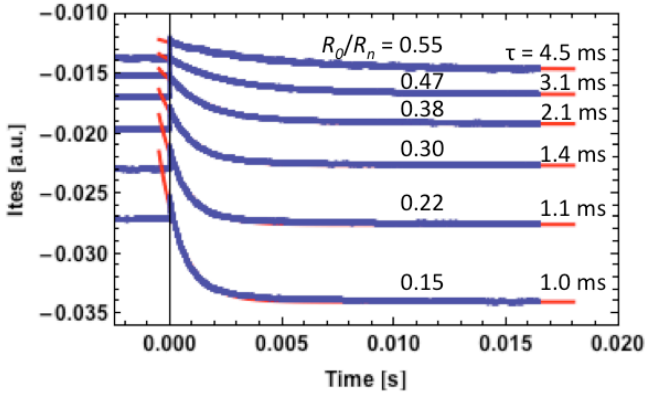

Fig. 6. The response signals (blue curves) to a small current bias step at different bias points. The fits (red curves) are first order exponential decay functions that give the time constants.

VI. Complex Impedance Measurement

For the complex impedance measurements we use a 10 kΩ resistance as a noise source. This noise is amplified and then added to the *dc* bias. Both the input noise signal and the output of the SQUID amplifier are recorded. The complex impedance of TES can be written as:

$$Z_{TES}(j\omega) = \frac{V_{AC}(j\omega)}{R_{loadAC} \cdot I_{TES}(j\omega)} \cdot T(j\omega) - Z_{Th}(j\omega) \cdot \quad (4)$$

where

$$Z_{Th}(j\omega) = R_{series} + R_{shunt} + j\omega L . \quad (5)$$

Here R_{loadAC} is the resistance in series with the noise source, R_{series} is the series resistance with the TES in the bias circuit , R_{shunt} is the shunt resistance and L is the inductance in the bias circuit. $T(j\omega)$ is the transfer function of the signal lines that is determined experimentally. In order to calculate the $Z_{TES}(j\omega)$ from (4) and (5), we need to find $T(j\omega)$ and L. All other parameters are known. These two can be calculated by using two equations for superconducting and normal state where Z_{TES} is known. At the superconducting state the $Z_{TES}(j\omega)$ is simply zero and at the normal state it is the normal resistance of the TES which is 103 mΩ in this case. The L obtain from this measurement is 0.5 μH.

Fig. 7 shows measured complex impedance curves different bias points in the transition at a bath temperature of 30 mK. In order to extract the TES parameters from the data we choose a simple, first order model that is described in great detail in Ref. [11]. In this model, the TES is seen as an isolated element with a certain heat capacity C that is connected to the bath with a low heat conductance G. In first order our device can be explained with this simple model especially in the low part of the transition where the complex impedance curves are very close to perfect semi-circle. In order to study these devices in greater detail more sophisticated models are needed that accounts for distributed heat capacities and heat conductance through the long legs.

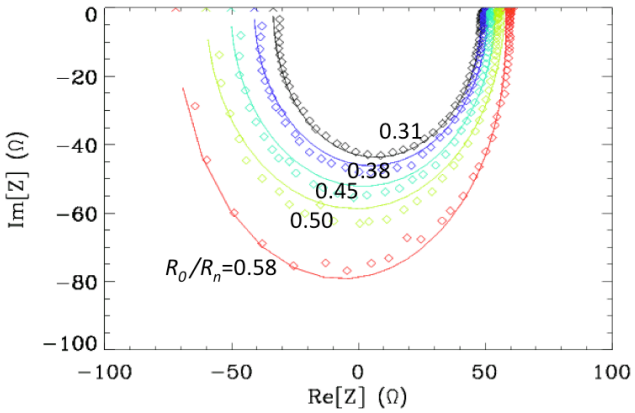

Fig. 7. Measured impedance at 5 points in the transition. R_0 is the TES resistance at the bias point where the impedance is measured and R_n is the normal state resistance of the device.

Using the electrical and thermal equations, the Z_{TES} can be written as:

$$Z_{TES} = Z_\infty + (Z_\infty - Z_0) \cdot \frac{1}{-1 + i\omega\tau_{eff}} . \quad (6)$$

, where Z_0 and Z_∞ are the impedances at zero and at very high frequency, respectively. τ_{eff} is the effective time constant, defined as:

$$\tau_{eff} = \tau_0 \frac{1+\beta+R_{th}/R_0}{1+\beta+R_{th}/R_0+(1-R_{th}/R_0)L_0}, \quad (7)$$

where $\tau_0 = C/G$ is the intrinsic time constant and L_0 is the low frequency loop gain that is: $L_0 = P_0\alpha/GT_0$. Here P_0 is the *dc* bias power and T_0 is the temperature of TES, which is close to T_C in the transition. α is the resistance dependence of the temperature at constant bias current. Similarly β is the resistance dependence of the current at constant temperature. These two are defined as:

$$\alpha = \frac{T_0}{R_0}\frac{\partial R}{\partial T}\bigg|_{I_0}, \quad \beta = \frac{I_0}{R_0}\frac{\partial R}{\partial I}\bigg|_{T_0}. \quad (8)$$

In this model Z_0 and Z_∞ become:

$$Z_0 = R_0\frac{1+\beta+L_0}{1-L_0} \quad (9)$$

$$Z_\infty = R_0(1+\beta) \quad (10)$$

By choosing the Z_0, Z_∞ and τ_{eff} at every bias point, (6) is fitted to the measured data. Knowing Z_∞ and R_0 we derived β from (10) and using that in (9), L_0 will be known. Knowing the loop gain (L_0) and effective time constant (τ_{eff}) and β, we calculate the intrinsic time constant (τ_0) from (7) and since the thermal conductance (G) is known from the IV measurement, we can estimate the thermal capacity (C) of the device.

Table 1 summarizes the outcome of this analysis for the TES in the transition at bias point where $R_0/R_n = 0.30$, which is a preferred operating point for these devices.

TABLE I DEVICE PARAMETERS FROM IMPEDANCE MEASUREMENT

TES parameter	Value
G	0.13 pW/K
C	2.3 fJ/K
τ_0	17.7 ms
τ_{eff}	1 ms
L_0	30
R_0	30 mΩ
P_0	3.8 fW
α	80
β	0.4

VII. CONCLUSION

We have fabricated and measured low thermal conductance TES devices as required for SPICA. We measured IV curves at different bath temperatures from 30 to 70 mK while it is mounted in a light-tight box to minimize the background load. The saturation power is 3.8 fW at 30 mK bath temperature. The thermal conductance extracted from the IV curves is 0.13 pW/K that corresponds to phonon noise NEP of 1.4×10^{-19} W/√Hz. However our noise measurement shows an electrical (dark) NEP of 4.2×10^{-19} W/√Hz. The reason for this excess noise is under investigation but we believe that the main part of this excess noise is due to the thermal fluctuations in the long legs. The complex impedance data can be relatively well described by a simple, first order model. We derive a heat capacity of 2.3 fJ/K and an effective time constant of about 1 ms when the TES is biased at $R_0/R_n = 0.30$ in the transition. The speed of the device is well below the specification for SPICA and can be further compromised by lowering the G to meet the sensitivity requirement.

ACKNOWLEDGMENT

We would like to thank all our collaborators within ESA-TRP program for fruitful discussions, specially P. Mauskopf, D. Morozov from Cardiff University, S. Withington, D. Goldie, D. Glowacka, A. Velichko from University of Cambridge, A. Murphy, N. Trappe, C. O'Sullivan from National University of Ireland in Maynooth, D. Griffin from Rutherford Appleton Laboratory and B. Leone from ESA.

REFERENCES

[1] H. Kaneda, T. Nakagawa, T. Onaka, T. Matsumoto, H. Murakami, K. Enya, H. Kataza, H. Matsuhara, and Y. Y. Yui, "Development of space infrared telescope for the SPICA mission," in Optical, Infrared, and Millimeter Space Telescopes. Edited by Mather, John C. Proceedings of the SPIE, Volume 5487, pp. 991-1000 (2004).

[2] B. Swinyard, "Esi: the far-infrared instrument for the spica mission," Space Telescopes and Instrumentation I: Optical, Infrared, and Millimeter 6265(1), p. 62650L, SPIE, 2006.

[3] B. Benson, S. Church, P. Ade, J. Bock, K. Ganga, C. Henson, and K. Thompson, "Measurements of Sunyaev-Zel'dovich effect scaling relations for clusters of galaxies," Astrophysical Journal 617, pp. 829–846, DEC 20 2004.

[4] G. W. Wilson, J. E. Austermann, T. A. Perera, K. S. Scott, P. A. R. Ade, J. J. Bock, J. Glenn, S. R. Golwala, S. Kim, Y. Kang, D. Lydon, P. D. Mauskopf, C. R. Predmore, C. M. Roberts, K. Souccar, and M. S. Yun, "The AzTEC mm-wavelength camera," Monthly Notices of the Royal Astronomical Society 386, pp. 807–818, MAY 11 2008.

[5] F. Piacentini, P. Ade, R. Bhatia, J. Bock, A. Boscaleri, P. Cardoni, B. Crill, P. de Bernardis, H. Del Castillo, G. De Troia, P. Farese, M. Giacometti, E. Hivon, V. Hristov, A. Iacoangeli, A. Lange, S. Masi, P. Mauskopf, L. Miglio, C. Netterfield, P. Palangio, E. Pascale, A. Raccanelli, S. Rao, G. Romeo, J. Ruhl, and F. Scaramuzzi, "The BOOMERANG North America instrument: A balloon-borne bolometric radiometer optimized for measurements of cosmic background radiation anisotropies from 0.degrees 3 to 4 degrees," Astrophysical Journal Supplement Series 138, pp. 315–336, FEB 2002.

[6] S. Masi, P. A. R. Ade, J. J. Bock, J. R. Bond, J. Borrill, A. Boscaleri, P. Cabella, C. R. Contaldi, B. P. Crill, P. de Bernardis, G. De Gasperis, A. de Oliveira-Costa, G. De Troia, G. Di Stefano, P. Ehlers, E. Hivon, V. Hristov, A. Iacoangeli, A. H. Jaffe, W. C. Jones, T. S. Kisner, A. E. Lange, C. J. MacTavish, C. M. Bettolo, P. Mason, P. D. Mauskopf, T. E. Montroy, F. Nati, L. Nati, P. Natoli, C. B. Netterfield, E. Pascale, F. Piacentini, D. Pogosyan, G. Polenta, S. Prunet, S. Ricciardi, G. Romeo, J. E. Ruhl, P. Santini, M. Tegmark, E. Torbet, M. Veneziani, and N. Vittorio, "Instrument, method, brightness, and polarization maps from the 2003 flight of BOOMERanG," Astronomy & Astrophysics 458, pp. 687–716, NOV 2006.

[7] M. Griffin, A. Abergel, P. Ade, P. Andr´e, J.-P. Baluteau, J. Bock, A. Franceschini, W. Gear, J. Glenn, D. Griffin, K. King, E. Lellouch, D. Naylor, G. Olofsson, I. Perez-Fournon, M. Rowan-Robinson, P. Saraceno, E. Sawyer, A. Smith, B. Swinyard, L. Vigroux, and G. Wright, "Herschel-SPIRE: design, performance, and scientific capabilities," in Space Telescopes and Instrumentation I: Optical, Infrared, and Millimeter. Proceedings of the SPIE, Volume 6265, pp. 62650A (2006).

[8] J.-M. Lamarre, J. L. Puget, M. Piat, P. A. R. Ade, A. E. Lange, A. Benoit, P. De Bernardis, F. R. Bouchet, J. J. Bock, F. X. Desert,

R. J. Emery, M. Giard, B. Maffei, J. A. Murphy, J.-P. Torre, R. Bhatia, R. V. Sudiwala, and V. Yourchenko, “Planck high-frequency instrument,” in IR Space Telescopes and Instruments. Edited by John C. Mather . Proceedings of the SPIE, Volume 4850, pp. 730-739 (2003).

[9] A. Turner, J. Bock, J. Beeman, J. Glenn, P. Hargrave, V. Hristov, H. Nguyen, F. Rahman, S. Sethuraman, and A. Woodcraft, “Silicon nitride micromesh bolometer array for submillimeter astrophysics,” Applied Optics 40, pp. 4921–4932, OCT 1 2001.

[10] P. D. Mauskopf, J. J. Bock, H. del Castillo, W. L. Holzapfel, and A. E. Lange, “Composite infrared bolometers with Si3N4 micromesh absorbers,” Applied Optics 36, pp. 765–771, Feb. 1997.

[11] M. A. Lindeman, S. Bandler, R. P. Brekosky, J. A. Chervenak, E. Figueroa-Feliciano, F. M. Finkbeiner, M. J. Li, and C. A. Kilbourne, Rev. Sci. Instrum. 75, 1283 2004.

[12] P. Khosropanah, B. Dirks, J. van der Kuur, M. Ridder, M. Bruijn, M. Popescu, H. Hoevers, J. R. Gao, D. Morozov, and P. Mauskopf, "Low Thermal Conductance Transition Edge Sensor (TES) for SPICA", AIP Conf. Proc. 1185, 42 (2009), DOI:10.1063/1.3292369

[13] D. Morozov, P. D. Mauskopf, P. Ade, M. Bruijn, P. A. J. de Korte, H. Hoevers, M. Ridder, P. Khosropanah, B. Dirks, and J.-R. Gao, "Ultrasensitive TES bolometers for space based FIR astronomy", AIP Conf. Proc. 1185, 48 (2009), DOI:10.1063/1.3292385

[14] P. Khosropanah, B.P.F. Dirks, M. Parra-Borderias, M. Ridder, R. Hijmering, J. van der Kuur, L. Gottardi, M. Bruijn, M. Popescu, J.R. Gao, H. Hoevers, "Transition Edge Sensors (TES) Using a Low-G Spider-Web-Like SiN Supporting Structure," *Applied Superconductivity, IEEE Transactions on*, vol.21, no.3, pp.236-240, June 2011.

[15] J. Mather, “Bolometer noise: nonequilibrium theory”, Appl. Opt. 21, 1125-1129 (1982).